ISSN 0006-3509, Biophysics, 2018, Vol. 63, No. 3, pp. 416–430. © Pleiades Publishing, Inc., 2018.
Original Russian Text © S.A. Kozhukhov, 2018, published in Biofizika, 2018, Vol. 63, No. 3, pp. 544–560.

CELL BIOPHYSICS

A Model of Temporal Encoding of Stimulus Orientation by Neuronal Responses in the Primary Visual Cortex

S. A. Kozhukhov*

Institute of Higher Nervous Activity and Neurophysiology, Russian Academy of Sciences, ul. Butlerova 5a, Moscow, 117485 Russia

**e-mail: serik1987@gmail.com*

Received July 3, 2017; in final form, November 23, 2017

Abstract—It has been shown experimentally that the stimulus orientation that elicits the optimal response in an orientation column in the primary visual cortex (area V1) undergoes rapid systemic changes that last 10–100 ms. These changes allow different orientation columns to encode information from multiple items in the visual space (the so-called temporal encoding). However, the mechanism of these changes is still unknown. In addition, most of the modern biophysical models are unable to reproduce these changes; the peak orientation of their responses is constant over time. In this paper, we suggest a method to improve the firing-rate ring model of the orientation hypercolumn by replacing the spatial symmetric distribution of local connections with a spatial anti-symmetric distribution. As a result, we obtained a more perfect model that is capable of reproducing such changes. Moreover, their amplitude is proportional to the extent of asymmetry in the spatial distribution of local connections.

Keywords: firing rate model for neural population, orientation tuning, dynamics, primary visual cortex, orientation column, short-range horizontal connections

DOI: 10.1134/S0006350918030119

Neurons of the primary visual cortex (V1) selectively respond to the bands or contours of a particular spatial orientation [1]. The concept of a selective response implies that at every instant a neuron elicits a relatively strong response only to a stimulus with a particular orientation. At the same time, it responds much less to other directions in space. The direction that causes such a relatively strong response in the cells is referred to as the peak orientation of a neuron.

Previously it has been shown [2–12] that such a peak orientation is temporally unstable: it can shift in a certain direction during response development: at some instant a stimulus can induce the optimal neuronal response; at another instant, the cell can be selective to quite another direction in space. Such changes were designated as the dynamics of peak orientation. They can be divided into a rapid type [3–12], with a characteristic time of approximately 10–100 ms, and a slow type [2], that lasts approximately 100–1000 ms. In this work we will consider only rapid changes in the peak orientation. Some authors believe [6, 13] that these changes increase the amount of information transferred by an orientation hypercolumn and, therefore, the transmission capacity of connections between different visual areas.

According to the data described in [6], such rearrangements are reproducible: they recur at each response to some stimuli; the values of their basic characteristics (amplitude, direction, and duration) do not vary during at least 5 h of an experiment and do not depend on the amount of anesthetic administered to an animal. In addition, studies [6, 7, 9, 10] showed that reliable dynamic shifts occur only in 50–70% of all neurons of area V1. Such neurons elicited stronger and less-selective responses compared to the cells with a stable peak orientation during a response [10].

Particular neurophysiological correlates of the shifts in peak orientation were revealed. In particular, they were shown [7] to be modified under the influence of intracortical inhibition, although inhibition per se was not the cause of their emergence. Nevertheless, the mechanism of these rearrangements is as yet unknown.

It can be expected [12] that these changes occur because one orientation column simultaneously accumulates the data on several spatial orientations obtained from the neighboring columns. Such accumulation requires a mechanism that would provide the propagation of visual signal and information transfer from one column to another. It has been shown [14, 15] that such a signal distribution is actually possible and that it has an autowave nature. In addition, model studies have shown [16, 17] that autowaves can occur solely due to excitatory horizontal connections. In light of the above, one can suggest that it is the short-

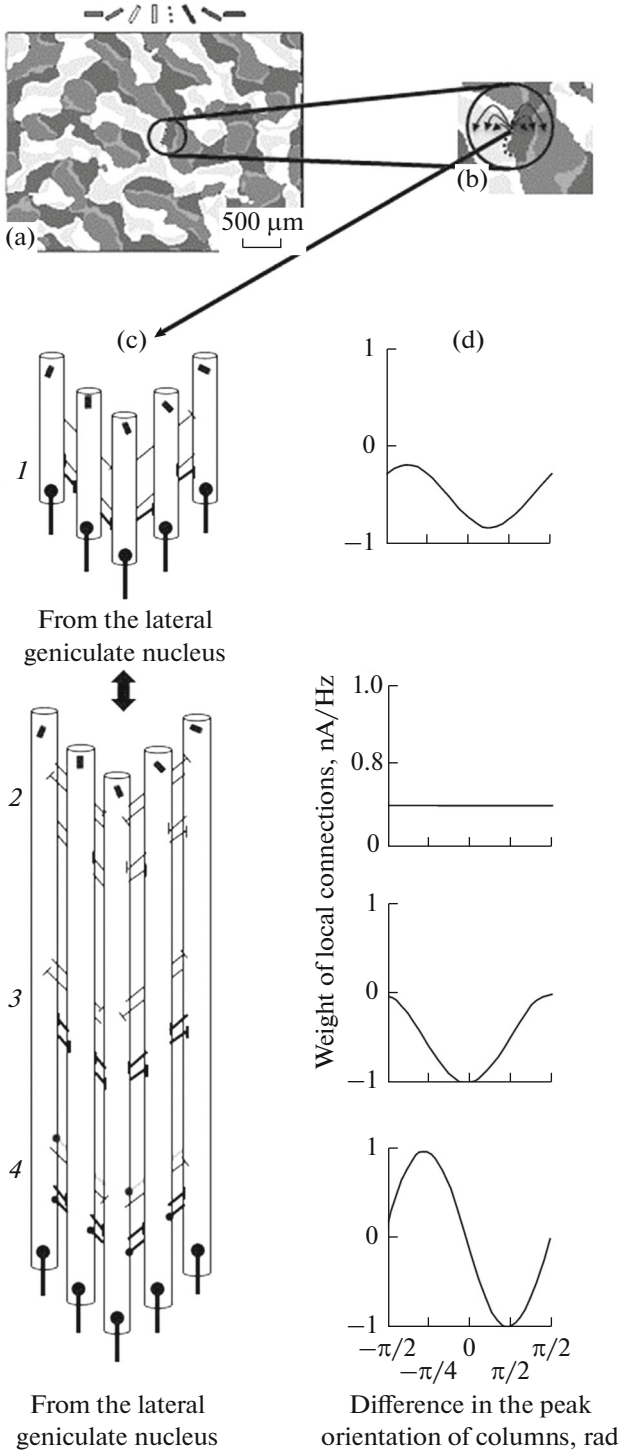

Fig. 1. The spatial structure of local connections in an area V1 orientation hypercolumn. (a) The functional map of V1 taken from [22]. (b) The enlarged image of the functional map section considered in the text. The dotted line shows the orientation column; the circle shows the supposed effective radius of short-range horizontal connections. Local connections are shown by arrows. (c) The presented systems of asymmetric local connections as a set of three subsystems operating in parallel and independently. The lines with a circle show the connections with prevalence of excitation; the lines with a stroke show the connections with prevalence of inhibition. The arrow thickness is proportional to the synaptic "weight" of the connection (the total magnitude of specific impact on the postsynaptic neuron). (d) An example of the spatial distribution of the weights of the system of local connections and its subsystems shown in (c). The difference between the preferred orientations of two columns is on the *X*-axis; the mean synaptic weight of local connections between these columns is on the *Y*-axis. In (c) and (d): (*1*) the configuration of the entire system of asymmetric local connections; (*2*) the configuration of its homogeneous component; (*3*) symmetric component; (*4*) anti-symmetric component.

range horizontal connections that lead to the dynamics of peak orientation.

To verify this assumption, let us consider the basic properties of these connections. They link any neighboring cortical areas at a distance of 300–500 μm from each other [18–20], easily crossing the boundaries of orientation columns and hypercolumns, as well as other functional modules in V1. Their important peculiarity is the *principle of local nonspecificity*, as was proved experimentally in [21]. This consists of the following: if two orientation columns are located at the same distance from a cortical area, their local connections with this area are absolutely identical and have no specificity. From the principle of local nonspecificity it follows that the properties of horizontal connections are influenced by the geometric characteristics of orientation columns, that is, the distance between them and their sizes. The latter, as follows from the results of optical mapping of the internal signal [18–20], are characterized by higher diversity: from several tens to several hundreds of microns. Small and large orientation modules very often adjoin each other, as is shown in Fig. 1a, in a circle. Due to such joining, the number of horizontal connections between two orientation columns depends not only on the difference of these columns but also on their location, as well as on the direction of these connections in space. In the example presented in Figs. 1a, 1b, the local connections directed leftwards are terminated at only one orientation column, while the connections directed rightwards are terminated at three columns. Such a property of local connections is called asymmetry.

The method of mathematical modeling is extensively used to describe the effects of local connections on orientation tuning and its potential modifications [23–28]. The available scientific literature offers a great diversity of models of the layer of the fourth orientation hypercolumn (pinwheel). Among these are both the more primitive one-dimensional model [23] and more-complex models, where a hypercolumn is a two-dimensional structure [24–26]. In addition, some studies were carried out with regard to the work of not only orientation detector neurons but also the detectors of spatial frequency [24] or color [28]. The functions of separate neurons or populations were described both by less realistic methods based on firing-rate population models [23, 24, 27] and by the more natural models based on the Hodgkin–Huxley equations in the original variant [25] and in terms of refractory density [26] and the Fokker–Planck equation [27]. Nevertheless, the common property of these models is their inability to reproduce the experimentally detected dynamic changes of the preferred orientations of neurons.

Such a discrepancy between experimental [6–12] and theoretical [23–28] data, in all likelihood, is associated with the following fact: in the above models it has been postulated that the local connections in V1 are radially symmetric, while in real hypercolumns they are asymmetric (Fig. 1b). It can be supposed that this asymmetry allows any column in area V1 to obtain information at a particular instant only from certain orientation columns, which can potentially lead to the shift of the peak orientation in a strictly definite direction. This work was aimed at testing this idea and constructing a neural network model on its basis.

To achieve this goal, it is proposed to improve the frequency population ring model of the orientation hypercolumn presented in [23] by replacing the radially symmetric system of connections with a more realistic asymmetric system. The analysis of the process of orientation tuning formation, as well as the changes in the peak orientation of its response in this model, will be considered below.

MODEL DESCRIPTION

The major structural unit of the improved V1 model is an orientation column. This is linked through afferent connections to neurons of the lateral geniculate nucleus and through local connections to the neighboring columns. Afferent connections induce a synaptic current that reaches its maximum in responses to a strictly definite orientation, which is referred to as the *preferred orientation* of the column.

The local connections link the neighboring columns, forming a system similar to that in Fig. 1c, *1*. The spatial distribution of the synaptic weights of these connections can be described as a certain continuous function (Fig. 1d, *1*). We can distribute this function to the sum of even and odd components, each of these is assigned to a particular group or subsystem of local connections (Figs. 1d, *2–4*). Eventually, our system of connections can be presented as an assembly of the following three subsystems (Fig. 1c):

1. The subsystem of homogenous connections described by a continuous function. These connections have no orientation specificity: they connect absolutely all columns without exception and their "weights" do not depend on the properties of the columns (Figs. 1c, *2*; 1d, *2*).

2. The subsystem of symmetric connections with spatial distribution described by an even function (Fig. 1d, *3*). Such connections are specific to the columns, but they are also isotropic: their "weights" depend only on the distance between two functional modules and on the difference between their preferred orientations but not on the direction of these connections in space (Fig. 1c, *3*).

3. The subsystem of anti-symmetric connections that correspond to the odd function (Fig. 1d, *3*). Such connections are not isotropic, but they are characterized by two highly unique properties (Figs. 1c, *4*; 1d, *4*): all excitatory connections are strictly ordered in a particular direction, while all inhibitory connections are strictly ordered in the opposite direction; the "weights" of excitatory connections (proportional to the arrow thickness in Fig. 1c) and the "weights" of

inhibitory connections are equal to each other in absolute values.

Complying with the ideas proposed in [23, 24, 27], we present the model as the following differential equation:

$$\tau_m \frac{\partial m}{\partial t} = -m + g\left\{ I[1 + C\cos(2\theta - 2\theta_0)]H(t) + \int_{-\frac{\pi}{2}}^{\frac{\pi}{2}} \frac{2d\theta'}{\pi} m(\theta', t) \times \left[\frac{1}{2}J_0 + J_2\cos(2\theta - 2\theta') + J_2^* \sin(2\theta - 2\theta')\right]\right\}, \quad (1)$$

where $m(\theta, t)$ is the activity of the column with the preferred orientation θ at time t; I and C are the brightness and contrast of the stimulus, respectively; J_0, J_2 and J_2^* are the characteristic weights of homogeneous, symmetric, and anti-symmetric connections, respectively; τ_m is the inertia of the neuronal population; θ_0 is the orientation of the presented stimulus; $H(t)$ is the Heaviside function, and $g(x)$ is a certain function described by the following equation:

$$g(x) = \begin{cases} \beta(x - T), & x \geq T, \\ 0, & x < T, \end{cases} \quad (2)$$

where T is the threshold value of the total synaptic current and β is the amplification factor. In our model, we have analyzed neuronal responses only to sufficiently bright stimuli, for which $I \gg T$. We also suppose that the activity of all neurons of our network at $t < 0$ is equal to zero.

This equation compactly describes the behavior of our neuronal network and all its properties. A further objective is to determine which of the contributions of each of the three subsystems of connections (the contributions, as we put it, are the βJ_0, βJ_2 and βJ_2^* values) are necessary for the above model to reproduce the key properties of real orientation hypercolumns in V1, namely: (a) the sharp orientation tuning amplified due to horizontal connections (see, e.g., [23–28]) and (b) the dynamics of the peak orientation of responses discovered in [6–12]).

In order to accomplish this task, we assessed the changes in peak orientation and tuning width (in our work, the tuning width is the width of the range of orientations that the column responds to) during response development. To assess the characteristic value of such changes, we determined the difference between the values of these two characteristics at the beginning of a response and at the end of a response. The values in the beginning of a response were determined as the values at the instant $t \to +0$, while those at the end of the response were determined by the properties of stable equilibrium states of the model. The analysis of these states will be considered in the next section.

A PARAMETRIC ANALYSIS OF THE PROPERTIES OF A NEURAL NETWORK

The detailed parametric analysis of equation (1) is described in the Supplement at the end of the article. Here, we will dwell on the results of this analysis. These are presented in Fig. 2.

As one can see from Fig. 2, the main parameters of the model that determine the properties of its stationary states are the contributions of each of the three subsystems of connections. The following four regimes of system function may occur depending on their ratio.

Regime A. This occurs under conditions of a relatively strong symmetric and weak homogeneous inhibition (Fig. 2a). In this regime, a cell elicits very weak orientation tuning with the half-width of 90 degrees. At the end of response, the orientation of the stimulus that causes the best response in the column (the so-called peak orientation) differs from its preferred orientation by the value $\Delta\theta_{PO}$, which is determined on the basis of the ratio:

$$\tan 2\Delta\theta_{PO} = -\frac{\beta J_2^*}{1 - \beta J_2^*}. \quad (3)$$

Regime B. This regime is possible at a certain balance between symmetric excitation and symmetric inhibition (Fig. 2b). Here, due to the work of horizontal connections, the width of orientation tuning narrows to the value θ_c^∞, which is implicitly defined by the ratios:

$$\begin{gathered} (1 - \beta J_2\gamma_1(\theta_c^\infty))^2 + (\beta J_2^*\gamma_1(\theta_c^\infty))^2 \\ = (\beta J_0\gamma_2(\theta_c^\infty) + \cos 2\theta_c^\infty)^2 C^2, \\ \beta J_0\gamma_2(\theta_c^\infty) + \cos 2\theta_c^\infty < 0, \end{gathered} \quad (4)$$

where C is the contrast of the stimulus; $\theta_1(\theta_c)$, $\gamma_2(\theta_c)$ are functions that are continuous and monotonously

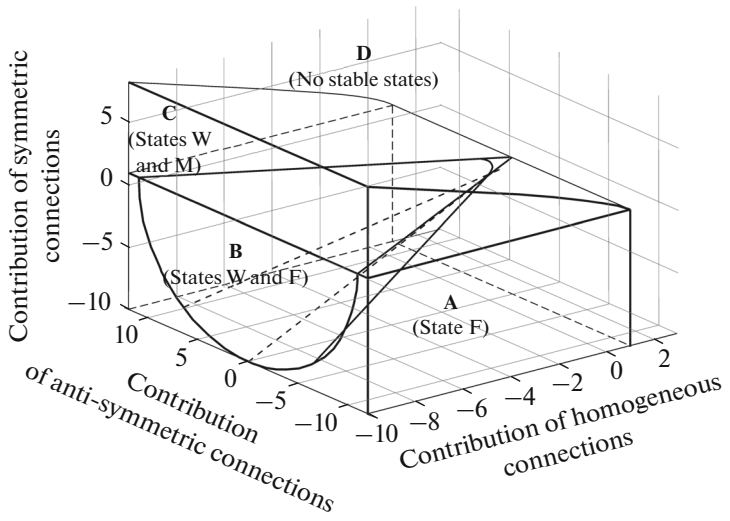

Fig. 2. The phase diagram of different stable stationary states of the model. On the axes: the contributions of some or other subsystems of connections (values βJ_0, βJ_2, βJ_2^*). There are four operating regimes altogether: the regime when the simulated neural network can be only in state F (A); in state F and state W (B); in state M and state W (C); the regime when no state of stable equilibrium is formed in response to any stimulus (D). The boundaries of the regimes given by condition (A-21) are omitted for clarity.

increasing at values $0 \le \theta_c \le \frac{\pi}{2}$; these take values from 0 to 1. Their analytical expression is given in the Supplement (equations (A-17)).

At the same time, the peak orientation at the end of response differs from the preferred orientation by a value defined as:

$$\tan 2\Delta\theta_{PO} = -\frac{\beta J_2^* \gamma_1(\theta_c^\infty(C))}{1 - \beta J_2 \gamma_1(\theta_c^\infty(C))}. \quad (5)$$

Let us note that all columns have the same neuronal activities in regimes A and B in the state of stable equilibrium corresponding to the background.

Regime C. This is possible in the case of moderate prevalence of excitation over inhibition (Fig. 2c). Here, after the responses to oriented stimuli ($C \neq 0$), the system is in the same equilibrium state as in regime B; however, in case of background presentation ($C = 0$), the equilibrium state with uniform distribution of neuronal activity will not already be stable. In the stable stationary cycle that occurs under these conditions the activity circulates around a ring and is spread as autowaves from one column to another with a definite speed. According to the data obtained in [29], such an autowave process is a model of visual hallucinations. Since it describes the behavior of a hypercolumn in the state of pathology it will not be considered below.

Regime D. In this case, there is a high prevalence of intracortical excitation (Fig. 2d). The major property of such a regime is that any equilibrium state is either unstable or absent during the presentation of oriented gratings. After the response, there is an avalanche-like increase in neuronal activity, which describes the initial stage of epileptic seizure well. This regime will not be considered in our work for similar reasons.

Symmetric and anti-symmetric connections play different roles in the formation of orientation tuning and rapid changes in peak orientation. Equation (4) specifies the width of orientation tuning for regime B. Its graphic representation in the space of contributions (βJ_0, βJ_2, βJ_2^*) is shown in Fig. 3. The surfaces presented in this figure correspond to the states where all columns at the end of the response have a definite tuning width, as indicated on the inserts. These graphs show the amplification of orientation tuning at increased contributions of symmetric and homogeneous connections. Such amplification was described in the models in [23–28] and was experimentally confirmed in numerous experimental works. We have shown that this is associated solely with the homogeneous and symmetric connections. In its turn, the increase in the contribution of anti-symmetric effects, on the contrary, results in lower selectivity of neurons. This means that anti-symmetric connections do not determine selectivity correction but play a different functional role.

In order to elucidate their role, let us examine how different types of horizontal interactions influence the changes in the peak orientation of response during its response. The level of such changes was calculated by formulas (3) and (5), which are graphically presented in Fig. 4. In this figure, any plane is a set of states of the orientation hypercolumn where the peak orientations of all columns are shifted during the response by the same amount, as indicated on the inserts. At the same

time, the central plane, which corresponds to the zero contribution of anti-symmetric connections, represents the set of states characterized by stable (invariable) peak orientation. The figure clearly shows that the main cause of changes in detector properties is the presence of anti-symmetric local connections: the higher their contributions are, the stronger the dynamic shifts are. At the same time, we can see in Fig. 4 that symmetric connections influence the dynamics only implicitly and indirectly: the change in their contribution leads only to the change in the coefficient of proportionality between parameter βJ_2^* and the size of the shifts $2\Delta\theta_{PO}$ but not the $2\Delta\theta_{PO}$ value per se. This means that anti-symmetric but not in any way symmetric connections are responsible for the changes in the optimal orientation of neuron.

Summarizing the results presented in Figs. 3 and 4, we can see that symmetric and anti-symmetric interactions perform different functions in V1. In addition, anti-symmetric connections per se are the mechanism of the formation of dynamics. In the next section, we will see how this mechanism works.

NUMERICAL SIMULATION OF NEURAL RESPONSES

We performed the numerical solution of equation (1) by the first-order Euler method. The time step was chosen to be 1 ms. Integration was carried out by the method of rectangles; the integration step was preset to be 0.1 rad. Numerical simulation was performed for the following values of parameters: $\beta = 1$ Hz/pA, $T = 5$ pA, $I = 100$ pA, $\tau_m = 20$ ms, $J_0 = -5$ pA/Hz, $J_2 = -5$ pA/Hz, and $J_2^* = -4$ pA/Hz. Unfortunately, due to the low precision of frequency–population neural network models, we obtained only the coarse and qualitative simplification of the function of real neural network. This discloses some, but far from all, aspects associated with the changes in peak orientations of responses. Let us consider such aspects in more detail.

Results of numerical simulation. The rough estimate of changes in the peak orientation of our model is shown in Fig. 5a. As the graph shows, the magnitude of these changes is 37.5°.

Figures 5b, 5c shows the very approximate work of the mechanism that causes such shifts. In this column, as the figures show, neural activity at the beginning of response is formed solely due to the afferent current (Fig. 5b, the dotted curve), because local connections have not yet been activated. The maximum value of this current is 175 pA; it is observed in responses to gratings with the orientation of 0° (Fig. 5b, *2*, the dotted curve). As a consequence, the initial tuning of the cell is formed exactly to horizontal gratings.

Hereafter, during development of a response, the peak orientation of this tuning will undergo substantial shifts caused by anti-symmetric connections. The configuration of such connections is shown in Fig. 5c. As this scheme shows, the column responsible for distinguishing the horizontal part (Fig. 5c, in the center) will be excited during most of the response by another column that selectively responds to the orientation of +45° (Fig. 5c, on the right). At the same time, the functional module responsible for the –45° grating (Fig. 5c, on the left) will mostly have an inhibitory effect.

How will it influence the activity in the 0° column? This will depend on the grating. If a horizontal grating is used, our column (Fig. 5c, in the center) will first activate the module responsible for the orientation of –45° (Fig. 5c, on the left); the latter, in turn, will inhibit it. This inhibition will result in the formation of a negative "local" current of high amplitude (Fig. 5b, *2*, the dashed line). As a result, the initially high activity of the column will gradually decrease (Fig. 5b, *2*, the solid line).

However, quite different processes will occur if the +45° grating is presented. In this situation, the column will be exposed to a strong anti-symmetric excitation by its neighbor with the preferred orientation of +45° (Fig. 5c, in the center and on the right). Such excitation will compensate for the inhibitory effect of symmetric and homogeneous connections by creating an actually zero "local" synaptic current (Fig. 5b, *1*, the dashed line). As a result, due to the effect of afferent excitation, the neural activity will mostly increase (Fig. 5b, *1*, the solid line).

Thus, we can see that there will be at least two opposite processes in our column after the formation of the initial tuning to the orientation of 0°: the decrease in neural activity in response to the horizontal grating (Fig. 5b, *2*) and its gradual increase in response to the diagonal of +45° (Fig. 5b, *1*). In 20–30 ms, these activities will become equal and it will correspond to the dynamic change in peak orientation by the magnitude of +45° (Fig. 5a).

Thus, we have shown that the main cause of changes in the peak orientation of V1 neurons is the "jump" of activity from one column to another, which allows the neurons of this column to respond to a particular stimulus in the same way that the neurons of the neighboring column did 10–20 ms ago. This is the main idea of our model.

DISCUSSION

Comparison with the existing models. The model of an orientation hypercolumn constructed in our work is an extension of the classical ring model [23], because the model described in our work and the classical model [23] are completely equivalent in the case of a zero contribution of anti-symmetric connections. As a consequence, it reproduces all events and effects that can be reproduced both in the model described in

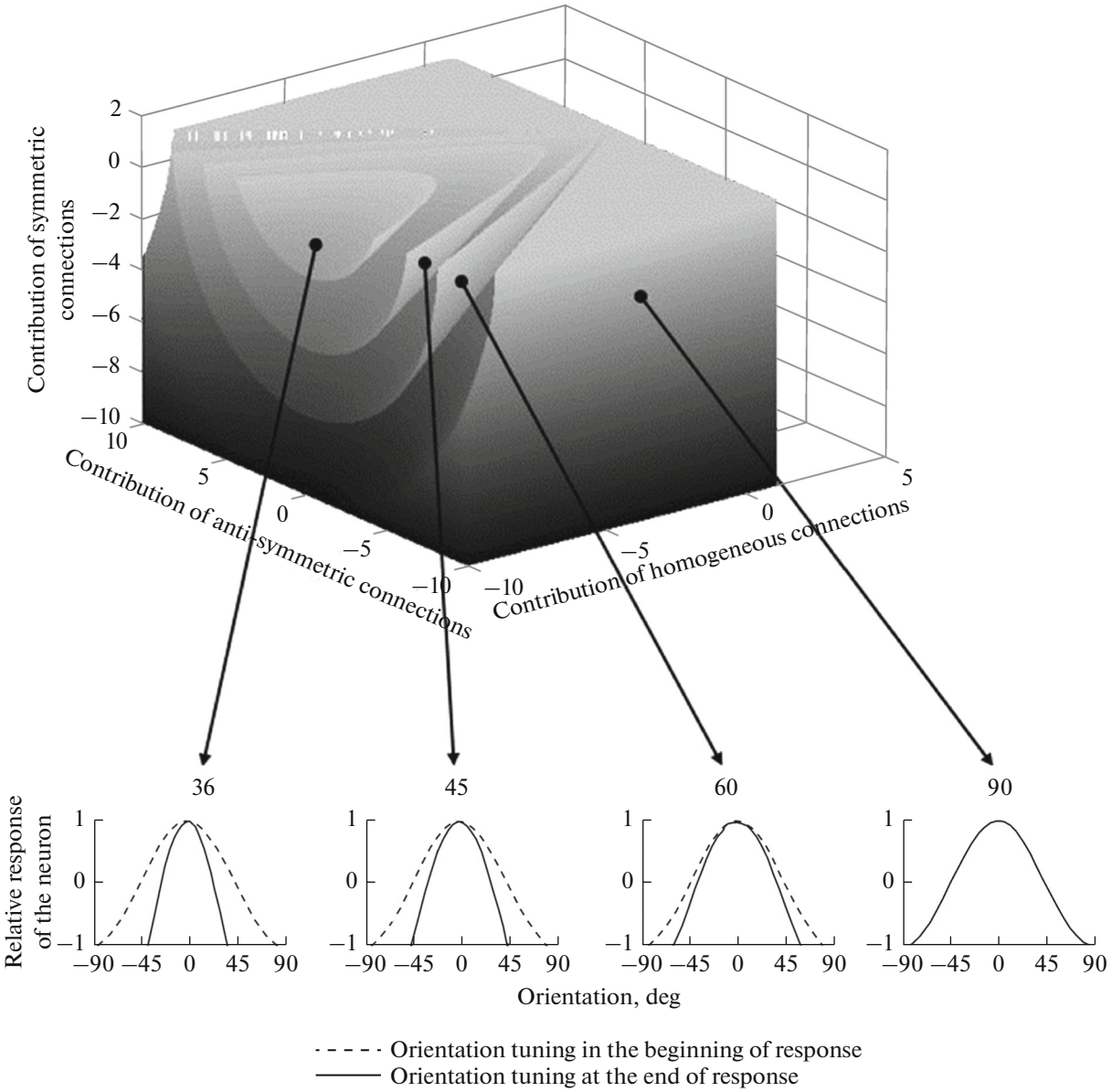

Fig. 3. The dependence of the width of orientation tuning on the contributions of three subsystems of local connections (βJ_0, βJ_2, and βJ_2^*). These contributions are shown on the *X*, *Y*, and *Z* axes. Each surface corresponds to numerous states characterized by the same width of orientation tuning indicated on the respective insert to the graph. On the same insert, dashed and solid lines show the tuning in the beginning of response and in the state of stable equilibrium, respectively.

[18] and in other analogous models [24–27]. Such effects can include, in particular, the sharpening of orientation tuning due to homogeneous and symmetric local connections and the presence of a stationary state with a low selectivity (regime A), as well as partial (regime C, or marginal state) and complete (regime D) loss in stability of the system at particular parameter values.

Let us also note that the optimal working parameters of the orientation hypercolumn in the model are the values in close proximity to the boundary of stability loss (Figs. 3 and 4). In other words, the better the detector neuron displays the local characteristic, the more easily its balance can be upset (i.e., the less reliable it is). These are rather interesting properties that have been also reproduced in other orientation hypercolumn models (see, e.g., [25]). They have yet to be verified experimentally.

Novel properties of our model. We have improved the classical model [23] by adding anti-symmetric connections (Fig. 1c, *4*; 1d, *4*). As a result of this improvement, the above properties were combined with new features associated with the work of these connections. The main feature is the rapid changes in the direction in space to which a neuron responds most optimally; in the available literature [6–12] such

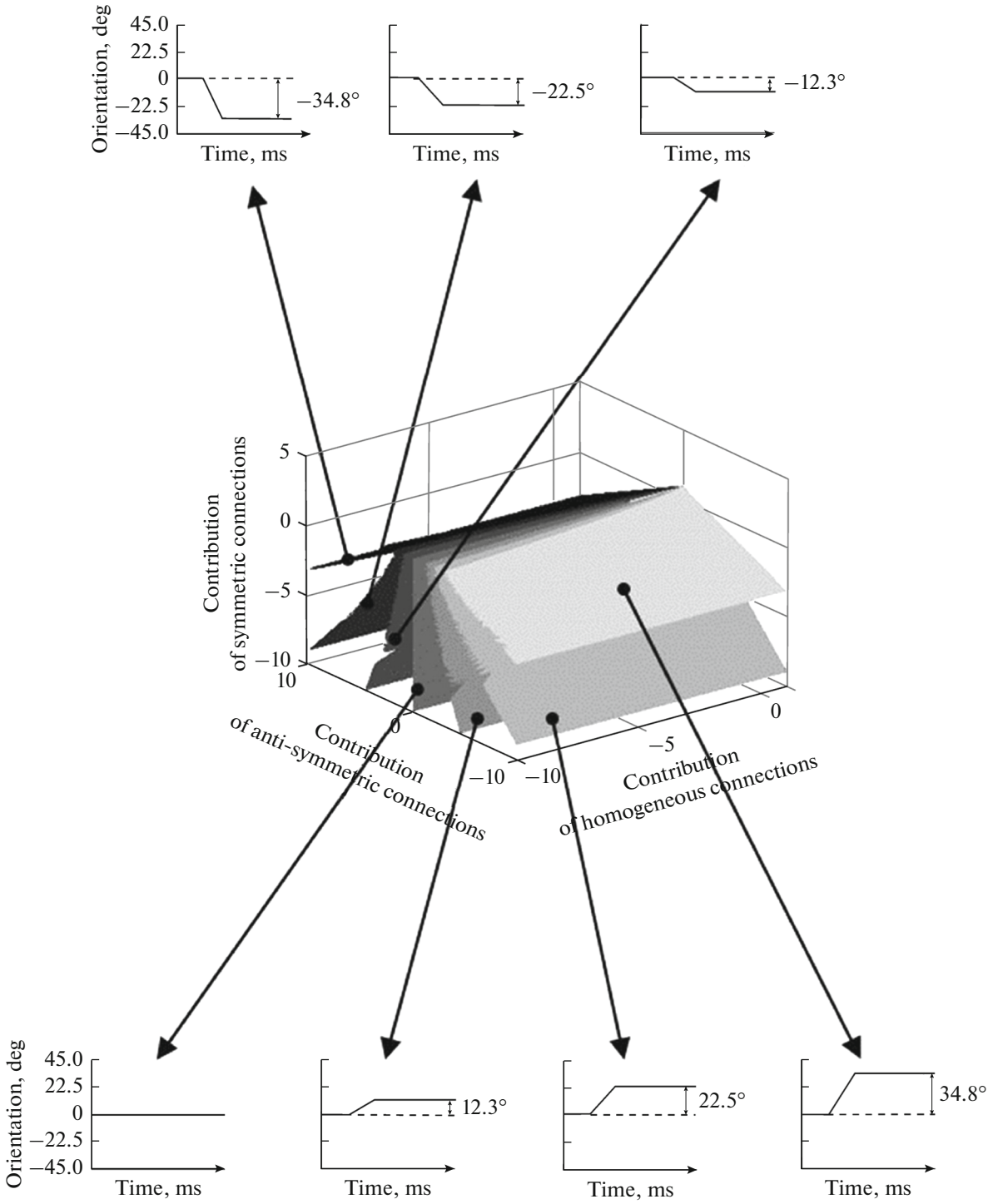

Fig. 4. The dependence of the total magnitude of the shift in preferred orientation on the contributions of three subsystems of local connections (βJ_0, βJ_2, and βJ_2^*). These contributions are shown on the *X*, *Y*, and *Z* axes. Each surface corresponds to numerous states with the particular magnitude of the total shift indicated on the respective insert. The same insert presents an example of dynamic changes with the same magnitude of dynamic shift. The situation with zero activity of all neurons of the network before the presentation of a stimulus is considered. A set of sinusoidal gratings with different orientations with the contrast $C = 1$ and the intensity $I = 300$ nA were used as a stimulus.

changes are referred to as the dynamics of the peak orientation (Fig. 5).

The comparison of theoretical and experimental data leads to a suggestion that these changes were studied in [6–12], as well as in [4, 5], because:

(a) On presentation of a band or a grating of a particular orientation, the peak orientation will be shifted by the $\Delta\theta_{PO}$ value, which is determined by the stimulus contrast (equation (5)) and the neural network parameters but does not depend on the preferred orientation of the neuron. At the same time, if the peak orientation is shifted at some values of the contrast, it will also be shifted at its other values. Analogous features are typical of the changes obtained experimentally in [6–12] (an example of experimental data described by the model is given in [9]).

(b) The neurons characterized by the changes in peak orientation ($J_2^* \neq 0$, $\Delta\theta_{PO} \neq 0$) have lower selectivity and lower response amplitude compared to the cells with stable peak orientation ($J_2^* = 0$, $\Delta\theta_{PO} = 0$): the model represents it in equations (5) and (A-19) (see also Fig. 4), while experimental data were obtained in [11].

(c) If a stimulus with the θ_1 orientation is presented after the response to a grating with the θ_2 orientation, the neural network will pass from the stationary state with the peak orientation of responses being $\theta_1 + \Delta\theta_{PO}$ into the state with $\theta_2 + \Delta\theta_{PO}$. As a consequence, the optimal response orientation per se in this case changes to the $\theta_2 - \theta_1$ value, depending only on the parameters of the present and preceding stimuli. This is in complete agreement with the experimental data reported in [4].

This model allows us to make certain assumptions about the main properties of the dynamics of peak orientation. These assumptions are given below.

(1) The lower the asymmetry in spatial configuration of orientation columns is, the smaller the magnitude of their dynamic shifts is. In particular, cells with stable dynamics may be prevalent in the places where this asymmetry is absent (e.g., in the centers of big columns).

(2) The existence of the dynamics of peak orientation leads to an increase in the volume of information contained in an individual neural response and not to an increase in the volume of information contained in responses formed by all neurons of the hypercolumn.

(3). In animals with an ill-defined or absent column orientation (e.g., in rats or rabbits) the peak orientation either does not change or changes slightly.

Are the rapid changes in peak orientation associated with the changes in perceived orientation? All changes in the peak orientation of neural responses in V1 can be divided into rapid changes that last less than 100 ms [3–12] and cause no changes in the visual image that is perceived, and slower changes, with the characteristic time of development being more than 100 ms [2, 30], which cause distortions of the perceived image known as the tilt aftereffect. The model described in this work can explain the rapid changes in peak orientation [4–12] but is unable to explain their slower rearrangements [2, 30], because the characteristic time of development of slow changes exceeds the characteristic time of response development in our model (τ_m in equation (1)). At the same time, the alternative model proposed in [2] describes the changes in perceived orientation. Here, the short-term rearrangements of afferent connections play the key role. Since the characteristic time of development of these rearrangements is approximately 100–1000 ms, such a model, in contrast, can describe slow [2, 30] but not rapid [4–12] changes in peak orientation. Combining both results, we can see that rapid [4–12] and slow [2, 30] changes in peak orientation are fundamentally different processes, as they are different in their properties, mechanisms, and functional significance.

The presumptive functional significance of asymmetric connections. As one can see, in the presence of asymmetry in spatial distribution, an orientation column "combines" the information processed by several neighboring columns (Fig. 5c) and encodes this information on the basis of two properties of the response: the value and position of its maximum (Fig. 5b, *1*, *2*). As a consequence, the cell response per se carries much more information than any of its integral characteristics (e.g., the total number of pulses per response). Such properties of the model agree with the properties of real hypercolumns found as a result of experiments [13]. It has been proposed [6, 13] that a single neuron of area V1 can transmit the information processed by several neighboring cells, in other words, it can perform the procedure of multiplexing a visual

Fig. 5. The visual description of the process of formation of changes in preferred orientation. The graphs in the figure (a) and (b) are constructed for the column with its own preferred orientation equal to 0°. (a) The dynamics of the preferred orientation; time is on the *X*-axis; differently oriented stimuli that induce the maximum response at a given time are on the *Y*-axis. (b) The post-stimulus histograms (thick solid line), as well as the dynamics of synaptic currents: total (thin solid line), induced by afferent connections (dots), and induced by local connections (thin dashed line). Different graphs correspond to responses to the gratings in front of them. Time is on the *X*-axis; current, pA (for simple curves; the left axis), or pulsation frequency, Hz (for boldface curves; the right axis) are on the *Y*-axis. (c) The configuration of anti-symmetric local connections for the orientation column shown in the figures (a) and (b) and for the neighboring columns. The arrows with dots show the connections with prevalence of excitation; the arrows with strokes show the connections with prevalence of inhibition. The stimuli that induce the maximum afferent current for a particular column are indicted in the inserts. The initial conditions and parameters of stimulation are the same as in Fig. 4.

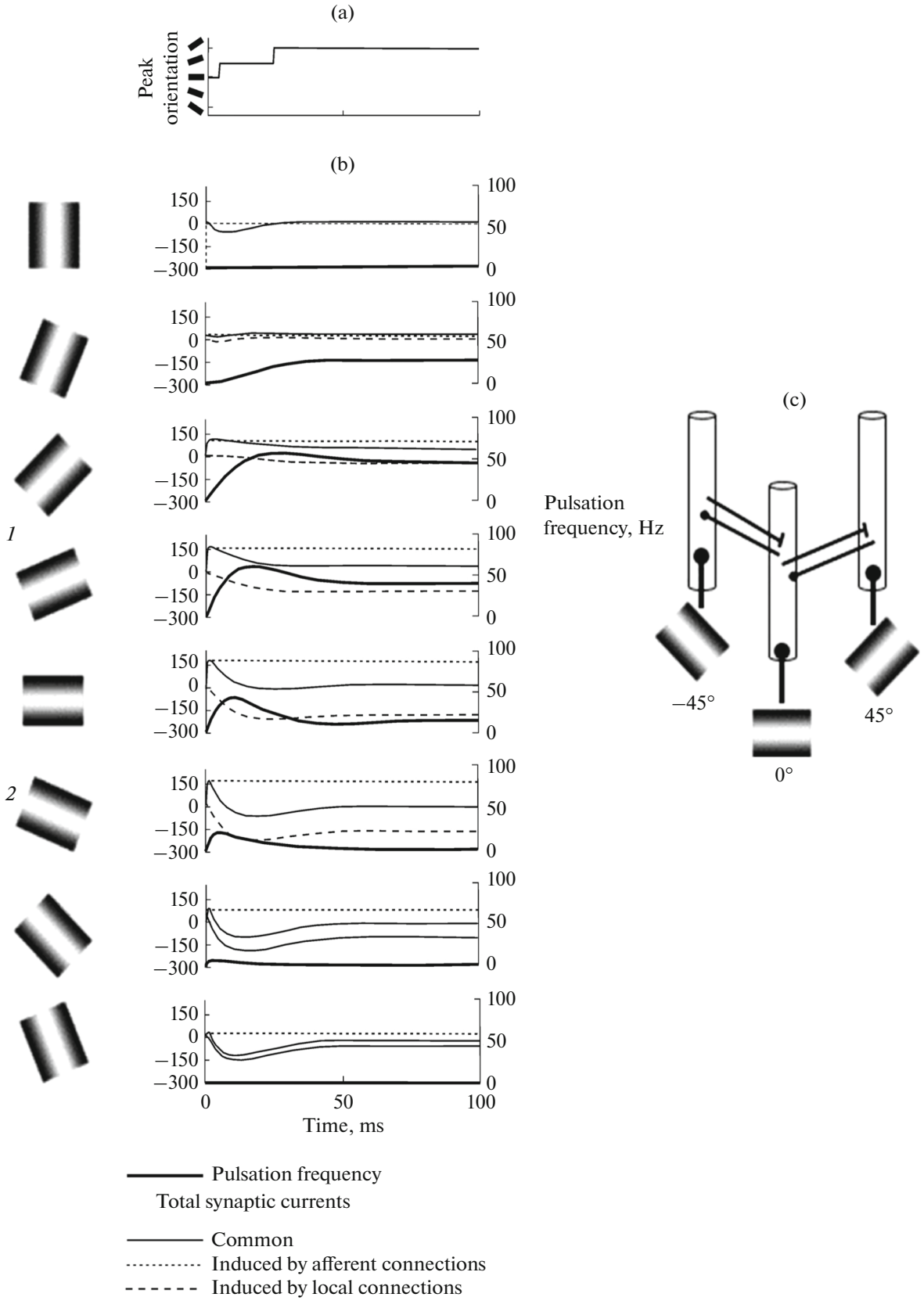
(a)
Peak orientation
(b)
150
0
–150
–300
100
50
0
1
2
0
50
100
Time, ms
(c)
Pulsation frequency, Hz
–45°
0°
45°
Pulsation frequency
Total synaptic currents
Common
Induced by afferent connections
Induced by local connections

signal. The significance of such multiplexing is probably that it contributes to minimizing the number of channels for transmitting visual information from V1 to the overlying areas.

CONCLUSIONS

The modernized ring model of layer 4 of an orientation hypercolumn with an asymmetric spatial distribution of local connections presented in Fig. 1c makes it possible to reproduce dynamic shifts in the preferred orientation of V1 neurons and to describe many experimental facts concerning these shifts in the framework of a single theoretical concept. We anticipate further development of this concept, primarily its application for improving two-dimensional orientation hypercolumn models.

APPENDIX

The Appendix presents a detailed description of the analysis of stable equilibrium states of the system, as well as the derivation of equations (3)–(6).

Simplification of the equation of the dynamics of neural activity. For simplicity and obviousness, let us consider the case of $t > 0$. Introducing the values $j_0 = \frac{1}{2}J_0,\ j_2 = \frac{1}{2}J_2 - \frac{1}{2}iJ_2^*,\ c = Ce^{-2i\theta_0}$, where i is the imaginary unit, and applying the Euler formula to all trigonometric functions of equation (1), we can present this equation as:

$$\tau_m \frac{\partial m}{\partial t} = -m + g \times \left\{ l\left[1 + \frac{1}{2}ce^{2i\theta} + \frac{1}{2}\bar{c}e^{-2i\theta}\right] + \int_{-\frac{\pi}{2}}^{\frac{\pi}{2}} \frac{2d\theta'}{\pi} m(\theta', t) \times \left[j_0 + j_2 e^{2i\theta - 2i\theta'} + \bar{j}_2 e^{2i\theta' - 2i\theta}\right] \right\}. \quad \text{(A-1)}$$

Let us expand the cell activity $m(\theta, t)$ into the Fourier series:

$$m(\theta, t) = \sum_{n=-\infty}^{+\infty} m_{2n}(t) e^{2in\theta},$$
$$m_{2n}(t) = \int_{-\frac{\pi}{2}}^{\frac{\pi}{2}} \frac{d\theta'}{\pi} m(\theta', t) e^{-2in\theta'}, \quad n \in \mathbb{Z}, \quad \text{(A-2)}$$
$$m_{-2n}(t) = \bar{m}_{2n}(t),$$

where $m_0(t)$, $m_2(t)$, $m_{-2}(t)$, ... are the respective expansion coefficients, the so-called harmonics. Equation $m_{-2n}(t) = \bar{m}_{2n}(t)$ follows from the fact that column activity $m(\theta, t)$ is a real quantity.

Let us then decompose the integral in (A-1) into separate summands and then substitute (A-2) into them:

$$\tau_m \frac{\partial m}{\partial t} = -m + g\left\{\left[l + 2j_0 m_0\right] + \left[\frac{1}{2}lc + 2j_2 m_2\right]e^{2i\theta} + \left[\frac{1}{2}\bar{l}\bar{c} + 2\overline{j_2 m_2}\right]e^{-2i\theta}\right\}, \quad \text{(A-3)}$$

Let us recall that in this equation $g(x)$ is the transfer function from the ratio (2) and the argument of this function is the total synaptic current $I(\theta, t)$. In order to expand $g(x)$, let us present this current as follows:

$$I(\theta, t) = \left[l + 2j_0 m_0\right] + 2\left|\frac{1}{2}lc + 2j_2 m_2\right|\cos(2\theta - 2\theta_p), \quad \text{(A-4)}$$

where $\theta_p(t)$ is the peak orientation of the column itself, whose total synaptic current is maximal at the given time under. This is defined as

$$2\theta_p = -\mathrm{Arg}\left[\frac{1}{2}lc + 2j_2 m_2\right]. \quad \text{(A-5)}$$

$I(\theta, t)$ takes the maximum value at $\theta = \theta_p$ and the minimum value at $\theta = \theta_p + \pi/2$. Let us write these values:

$$I_{\max}(t) = l + 2j_0 m_0 + 2\left|\frac{1}{2}lc + 2j_2 m_2\right|,$$
$$I_{\min}(t) = l + 2j_0 m_0 - 2\left|\frac{1}{2}lc + 2j_2 m_2\right|. \quad \text{(A-6)}$$

According to equations (1) and (2), only the columns with $I \geq T$ will participate in the formation of neuronal activity pattern. There are three possible cases depending on the relationships between the $I_{\max}$, $I_{\min}$ and T values.

1. **Case F.** This is possible when the synaptic current in all columns is above the threshold:

$$I > I_{\min} = l + 2j_0 m_0 - 2\left|\frac{1}{2}lc + 2j_2 m_2\right| \geq T. \quad \text{(A-7)}$$

Here, the $g(x)$ expression from equation (2) is expanded as follows:

$$\tau_m \frac{\partial m}{\partial t} = -m + \beta\left\{\left[l - T + 2j_0 m_0\right] + \left[\frac{1}{2}lc + 2j_2 m_2\right]e^{2i\theta} + \left[\frac{1}{2}\bar{l}\bar{c} + 2j_2 m_2\right]e^{-2i\theta}\right\}. \quad \text{(A-8)}$$

2. **Case C.** $I_{\max} \geq T \geq I_{\min}$. Here, the maximum synaptic current exceeds the threshold, while the minimum synaptic current does not:

$$I_{\min} = l + 2j_0 m_0 - \left|\frac{1}{2}lc + 2j_2 m_2\right| \leq T \leq l + 2j_0 m_0 + \left|\frac{1}{2}lc + 2j_2 m_2\right| = I_{\max}.$$

In this case, some orientation columns achieve a suprathreshold level of excitation and therefore are

active, while other columns achieve a subthreshold level of excitation and therefore are "silent." These are separated by columns with the synaptic current equal to the T threshold. Let us denote their preferred orientations as $\theta_p \pm \theta_c$. We then have a ratio following from expression (A-4):

$$I(\theta_p \pm \theta_c, t) = l + 2j_0 m_0 + 2\left|\frac{1}{2}lc + 2j_2 m_2\right|\cos(\pm 2\theta_c) = T. \quad \text{(A-9)}$$

Equation (5) for regime C takes the form of

$$\tau_m \frac{\partial m}{\partial t} = -m + \begin{cases} \beta\left\{[l - T + 2j_0 m_0] + \left[\frac{1}{2}lc + 2j_2 m_2\right]e^{2i\theta} + \left[\overline{\frac{1}{2}lc + 2j_2 m_2}\right]e^{-2i\theta} - T\right\}, & |\theta - \theta_p| < \theta_c, \\ 0, & |\theta - \theta_p| \geq \theta_c. \end{cases} \quad \text{(A-10)}$$

3. If all of the columns achieve a subthreshold level of excitation, then no activity is generated in the neural network:

$$I < I_{\max} = l + 2j_0 m_0 + \left|\frac{1}{2}lc + 2j_2 m_2\right| \leq T.$$

Such a case is possible only during the presentation of low-intensity stimuli or in their absence:

$$l(1 + C) \leq T.$$

The analysis of stable equilibrium states for case F. Let us differentiate $m_0(t)$, $m_2(t)$ from equations (A-2) by time and substitute the result of this operation into (A-8), taking the ratio $l \gg T$ into account:

$$\tau_m \frac{\partial m_0}{\partial t} = -(1 - \beta J_0)m_0 + \beta l, \quad \tau_m \frac{\partial m_2}{\partial t} = -(1 - 2\beta j_2)m_2 + \frac{1}{2}\beta lc. \quad \text{(A-11)}$$

By equating the left parts of equations (A-11) to zero, we will find the only stationary point for case F given by the equilibrium values of harmonics m_0^∞, m_2^∞:

$$m_0^\infty = \frac{\beta l}{1 - \beta J_0}, \quad m_2^\infty = \frac{\beta lc}{2(1 - 2\beta j_2)}. \quad \text{(A-10)}$$

Let us denote this stationary point as state F. In this state, a cell has the maximally broad orientation tuning, the half-width is equal to $\pi/2$.

Let us find the shift in peak orientation during the time of response development. For this purpose, let us write the spatial distribution of neuronal activity in state F. We can obtain it by substituting (A-12) into (A-2) and taking the ratio (A-5) into account:

$$m^\infty(\theta) = m_0^\infty + m_2^\infty e^{2i\theta} + \overline{m_2^\infty} e^{-2i\theta} = \frac{\beta l}{1 - \beta J_0} + \frac{\beta lC}{|1 - 2\beta j_2|}\cos[2\theta - 2\theta_0 - \mathrm{Arg}(1 - 2\beta j_2)].$$

Now, to find the peak orientation of the column at the end of the response (in the state of stable equilibrium) it is necessary to determine the values of the grating orientation θ_0 where the activity of the column with preferred orientation equal toθ will have a maximum value. For this purpose, let us differentiate the above expression with respect to θ_0 and equate the result of this operation to zero. Eventually, we will have:

$$2\Delta\theta_{PO} = \theta_0\big|_{\frac{\partial m^\infty}{\partial \theta_0} = 0} - \theta = -\mathrm{Arg}(1 - 2\beta j_2),$$

where $\Delta\theta_{PO}$ is the difference between the peak orientation at the end of the response and the preferred orientation of the column. After simplifying this expression, we will finally have equation (3).

Now, let us determine the boundaries of existence of state F. For this purpose, let us substitute equations (A-12) into condition (A-7) and take the fact into account that $l \gg T$ (we present the stimuli substantially above the threshold):

$$(1 - \beta J_2)^2 + (\beta J_2^*)^2 > (1 - \beta J_2)^2 C^2, \quad \beta J_0 < 1. \quad \text{(A-13)}$$

Finally, let us find the boundaries of stability of this state. For this purpose let us write the characteristic equation for (A-11):

$$\begin{vmatrix} \beta J_0 - (\lambda + 1) & 0 & 0 \\ 0 & \beta J_2 - (\lambda + 1) & -\beta J_2^* \\ 0 & \beta J_2^* & \beta J_0 - (\lambda + 1) \end{vmatrix} = 0,$$

where λ is the eigenvalues of the system.

If we expand the determinant of the matrix on the left and find the roots of the characteristic equation we will see that the area of stability characterized by $\lambda < 0$ is determined by the following conditions:

$$\beta J_0 < 1, \quad \beta J_2 < 1. \quad \text{(A-14)}$$

The area in the space of parameters described by equations (A-13) and (A-14) is marked in Fig. 2a. The operation of the neural network in this regime will be referred to as system functioning in regime A.

Stable stationary points and cycles for case C. To search for the states of stable equilibrium in case C it is necessary to replace the value T in the equation for the dynamics of activity (A-10) by the left part of equality (A-9) and then to simplify the result:

$$\tau_m \frac{\partial m}{\partial t} = -m + \begin{cases} 2\beta\left|\frac{1}{2}lc + 2j_2m_2\right|[\cos(2\theta - 2\theta_p) - \cos 2\theta_c], & |\theta - \theta_p| < \theta_c, \\ 0, & |\theta - \theta_p| \geq \theta_c. \end{cases} \quad \text{(A-15)}$$

Now, by differentiating the $m_0(t)$, $m_2(t)$ values from expression (A-2) with respect to time and substituting the obtained derivatives into expression (A-15), we derive the following equations that describe their dynamics:

$$\begin{aligned} \tau_m \frac{\partial m_0}{\partial t} &= -m_0 + 2\beta\left|\frac{1}{2}lc + 2j_2m_2\right|\gamma_2(\theta_c), \\ \tau_m \frac{\partial m_2}{\partial t} &= -m_2 + \beta\left(\frac{1}{2}lc + 2j_2m_2\right)\gamma_1(\theta_c), \end{aligned} \quad \text{(A-16)}$$

where $\gamma_1(\theta_c)$, $\gamma_2(\theta_c)$ are the first and second transcendent functions, respectively. They are determined by the following conditions:

$$\begin{aligned} \gamma_1(\theta_c) &= \frac{2\theta_c}{\pi} - \frac{\sin 4\theta_c}{2\pi}, \\ \gamma_2(\theta_c) &= \frac{\sin 2\theta_c - 2\theta_c \cos 2\theta_c}{2\pi}. \end{aligned} \quad \text{(A-17)}$$

These two functions at $0 \leq \theta_c \leq \pi/2$ take the values over the interval of [0; 1] and are monotonously increasing.

The stationary states of the system are determined on the basis of equations (A-16) and condition (A-9):

$$\begin{aligned} 2j_0m_0^\infty + l + 2\left|\frac{1}{2}lc + 2j_2m_2^\infty\right|\cos 2\theta_c^\infty &= T, \\ m_0^\infty &= 2\beta\left|\frac{1}{2}lc + 2j_2m_2^\infty\right|\gamma_2(\theta_c^\infty), \\ (1 - 2\beta j_2\gamma_1(\theta_c^\infty))m_2^\infty &= \frac{1}{2}\beta lc\gamma_1(\theta_c^\infty), \end{aligned} \quad \text{(A-18)}$$

where θ_c^∞ is the value of the critical angle in the equilibrium state. The left part of the latter equation implies the need to consider a general case corresponding to condition $1 - 2\beta j_2\gamma_1(\theta_c^\infty) \neq 0$ and a special case, for which equation $1 - -2\beta j_2\gamma_1(\theta_c^\infty) = 0$ is true. Let us denote these as case W and case M, respectively.

Case W. This occurs when one of the inequalities is fulfilled: $\beta J_2\gamma_1(\theta_c^\infty) \neq 1$, $\beta J_2^* \neq 0$. In this situation, we can divide both parts of the latter equation in expressions (A-18) by the value $1 - 2\beta j_2\gamma_1(\theta_c^\infty)$ and see that this case will also correspond to a single stationary state:

$$\begin{aligned} m_0^\infty &= \frac{\beta lC\gamma_2(\theta_c^\infty)}{\left|1 - 2\beta j_2\gamma_1(\theta_c^\infty)\right|}, \\ m_2^\infty &= \frac{\beta lC\gamma_1(\theta_c^\infty)}{2(1 - 2\beta j_2\gamma_1(\theta_c^\infty))}. \end{aligned} \quad \text{(A-19)}$$

Let us denote this as **state W**. The value of the critical angle θ_c^∞ here is found by substituting the values of (A-19) into equations (A-9). As a result of these operations, we obtain equation (4). The critical angle θ_c^∞ given by this equation corresponds to the half-width of orientation tuning. In the (βJ_0, βJ_2, βJ_2^*) coordinates, equation (4) will describe a conical surface that characterizes numerous states that correspond to a particular value of θ_c. For different values of θ_c, different conical surfaces are given which, in turn, will be located inside the cone determined by the following inequalities:

$$\begin{aligned} (1 - \beta J_2)^2 + (\beta J_2^*)^2 < (1 - \beta J_2)^2C^2, \\ \beta J_0 < 1. \end{aligned} \quad \text{(A-20)}$$

This will be the area of existence of stationary state W. The boundaries of this area in the space of parameters at $C = 1$ of the neural network are indicated in Fig. 2b. Let us denote such area as *regime B*. Let us note that if a low-contrast stimulus is presented, then, even in regime B the system will reach state F but not state W, as can be seen from equations (A-13) and (A-20).

The activity of orientation column in this state is found by substituting the stationary values of harmonics from (A-19) into (A-2) and taking the ratio (A-5) into account:

$$m^\infty(\theta;\theta_0) = \frac{lC}{\left|1 - 2\beta j_2\gamma_1(\theta_c)\right|} \times\left\{\cos(2\theta - 2\theta_0 - \mathrm{Arg}(1 - 2\beta j_2\gamma_1(\theta_c^\infty))) - \cos 2\theta_c\right\}_+,$$

where

$$\{x\}_+ = \begin{cases} 0, & x < 0, \\ x, & x \geq 0. \end{cases}$$

As in state F, the shift in preferred orientation of the column during the time of response development in state W is found by differentiating $m^\infty(\theta;\theta_0)$ with respect to θ_0 and equating the resulting expression to zero. As a result, we will obtain equation (5).

Now, let us determine the conditions where this stationary state will be stable. For this purpose, let us

make the following substitution in equations (A-14) and (A-9):

$$z = \beta\left(2j_2m_2 + \frac{1}{2}lc\right) = |z|e^{2i\theta_z}.$$

The result of this substitution is

$$2\beta j_0 m_0 + \beta l + 2|z|\cos 2\theta_c = \beta T,$$

$$\tau_m \frac{\partial m_0}{\partial t} = -m_0 + 2|z|\gamma_2(\theta_c),$$

$$\tau_m \frac{\partial |z|}{\partial t} = (\beta J_2 m_2(\theta_c) - 1)|z| + \frac{1}{2}\beta lC\cos(2\theta_c + 2\theta_z),$$

$$\tau_m\left[2|z|^{\infty}\frac{\partial \theta_z}{\partial t}\right] = -\beta J_2^*\gamma_1(\theta_c)|z|^{\infty} - \frac{1}{2}\beta lC\frac{|z|^{\infty}}{|z|}\sin(2\theta_0 + 2\theta_z).$$

Let us substitute $\theta_c(t) = \theta_c^{\infty} + \delta\theta_c$; $m_0(t) = m_0^{\infty} + \delta m_0$; $|z|(t) = |z|^{\infty} + \delta|z|$; $\theta_z(t) = \theta_z^{\infty} + \delta\theta_z$ into this equation and linearize the obtained system:

$$\tau_m \frac{\partial \delta m_0}{\partial t} = \left(\beta J_0\frac{2\theta_c^{\infty}}{\pi} - 1\right)\delta m_0 + \frac{2\sin 2\theta_c^{\infty}}{\pi}\delta|z|,$$

$$\tau_m \frac{\partial \delta|z|}{\partial t} = \beta_2 J_0 J_2\frac{\sin 2\theta_c^{\infty}}{\pi}\delta m_0 + \left[\beta J_2\left(\frac{2\theta_c^{\infty}}{\pi} + \frac{\sin 4\theta_c^{\infty}}{2\pi}\right) - 1\right]\delta|z| + \beta J_2^*\gamma_1(\theta_c^{\infty})\left[2|z|^{\infty}\delta\theta_z\right],$$

$$\tau_m \frac{\partial\left[2|z|^{\infty}\delta\theta_z\right]}{\partial t} = -\beta^2 J_0 J_2^*\frac{\sin 2\theta_c^{\infty}}{\pi}\delta m_0 - \beta J_2^*\left(\frac{2\theta_c^{\infty}}{\pi} + \frac{\sin 4\theta_c^{\infty}}{2\pi}\right)\delta|z| + \left[\beta J_2\gamma_1(\theta_c^{\infty}) - 1\right]2|z|^{\infty}\delta\theta_z.$$

By writing the characteristic equation for this linearized system we will obtain the following conditions of stability of the stationary state:

$$(\lambda+1)^3 - \left(\beta J_0\frac{2\theta_c^{\infty}}{\pi} + \beta J_2\frac{4\theta_c^{\infty}}{\pi}\right)(\lambda+1)^2 + \left[\beta^2 J_0 J_2\left(\frac{8\theta_c^{\infty 2}}{\pi^2} - \frac{2\sin^2 2\theta_c^{\infty}}{\pi^2}\right) + \beta^2|2j_2|^2\gamma_1(\theta_c^{\infty})\left(\frac{2\theta_c^{\infty}}{\pi} + \frac{\sin 4\theta_c^{\infty}}{2\pi}\right)\right](\lambda+1) \quad \text{(A-21)}$$

$$+ \beta^3 J_0|2j_2|^2\gamma_1(\theta_c^{\infty})\left(\frac{2\sin^2\theta_c^{\infty}}{\pi^2} - \frac{4\theta_c^{\infty 2}}{\pi^2} - \frac{\theta_c^{\infty}\sin 4\theta_c^{\infty}}{\pi^2}\right) = 0,$$

$$\mathrm{Re}\,\lambda < 0.$$

The numerical solution of equation (A-19) was found for each of the points used in making graphs in Figures 2–4. All points that do not satisfy the condition $\mathrm{Re}\,\lambda < 0$ were removed from the graphs.

Case M. For this case, the ratio $\beta J_2\gamma_1(\theta_c) = 1$ is fulfilled. According to equalities (A-18), this is possible only when $c = 0$. In other words, the stationary state corresponding to such a case does not exist in the responses to high-contrast gratings. Let us substitute the condition $c = 0$ into equations (A-16):

$$\tau_m \frac{\partial m_0}{\partial t} = -m_0 + 4\beta|j_2 m_2|\gamma_2(\theta_c),$$

$$\tau_m \frac{\partial m_2}{\partial t} = -m_2 + 4\beta j_2 m_2\gamma_1(\theta_c).$$

In the last of these equations, we will substitute $m_2 = |m_2|e^{2i\theta_2}$ and multiply the result by $e^{-2i\theta_2}$:

$$\tau_m \frac{\partial m_0}{\partial t} = -m_0 + |4\beta j_2||m_2|\gamma_2(\theta_c),$$

$$\tau_m \frac{\partial |m_2|}{\partial t} = [\beta J_2\gamma_1(\theta_c) - 1]|m_2|, \quad \text{(A-22)}$$

$$\tau_m \frac{\partial(2\theta_2)}{\partial t} = -\beta J_2^*\gamma_1(\theta_c).$$

If we equate the left parts of equations (A-22) to zero and substitute the result into (A-9) we can see that only one stationary regime of system operation is possible in case M, which is found as

$$|m_2|^{\infty} = -\frac{l}{4|j_2|(\beta J_0\gamma_2(\theta_c^{\infty}) + \cos 2\theta_c^{\infty})} \neq 0,$$

$$m_0^{\infty} = -\frac{\beta l\gamma_2(\theta_c)}{\beta J_0\gamma_2(\theta_c^{\infty}) + \cos 2\theta_c^{\infty}}, \quad \gamma_1(\theta_c^{\infty}) = \frac{1}{\beta J_2},$$

$$2\theta_2(t_2) = 2\theta_2(t_1) - \beta J_2^*\gamma_1(\theta_c^{\infty})\frac{t_2 - t_1}{\tau_m}, \quad t_1, t_2 \gg \tau_m,$$

where t_1, t_2 is the time that passes after presentation of the stimulus. The conditions of existence of case M follow from these equations. These are represented parametrically by the following inequalities:

$$0 \le \theta_c \le \frac{\pi}{2}, \quad \beta J_2 = \frac{1}{\gamma_1(\theta_c^{\infty})} > 1, \quad \beta J_0 < -\frac{\cos 2\theta_c^{\infty}}{\gamma_2(\theta_c^{\infty})}, \quad \text{(A-23)}$$

where $\gamma_1(x)$, $\gamma_2(x)$ are the functions determined by the ratio (A-15). All these equations determine the area in the space of neural network parameters, whose boundaries are shown in Fig. 2c.

In such a regime, the θ_2 value does not tend to a certain equilibrium value at $t \to +\infty$; instead, it changes with a constant rate at invariable $|m_2|^{\infty}$. Such changes are described on the phase plain as a closed curve. These are the stationary oscillations of the

$\mathrm{Re}m_2$ and $\mathrm{Im}m_2$ values corresponding to periodic oscillations of neuronal activity in each column. These oscillation processes circulate over the entire orientation hypercolumn, jumping from one module to another, and are referred to as a stationary cycle. Let us denote it as cycle M.

Let us determine the conditions when this stationary cycle will be stable. For this purpose, let us substitute the conditions $\theta_c(t) = \theta_c^\infty + \delta\theta_c$; $m_0(t) = m_0^\infty + \delta m_0$; $|m_2|(t) = |m_2|^\infty + \delta|m_2|$ into equations (A-22) and linearize the resulting system:

$$\tau_m \frac{\partial \delta m_0}{\partial t} = \left(\beta J_0 \frac{2\theta_c^\infty}{\pi} - 1\right)\delta m_0 + \beta|2j_2|\frac{2\sin 2\theta_c^\infty}{\pi}\delta|m_2|,$$

$$\tau_m \frac{\partial \delta|m_2|}{\partial t} = \frac{\beta J_0 J_2}{|2j_2|}\frac{\sin 2\theta_c^\infty}{\pi}\delta m_0 + \left(\beta J_2 \frac{4\theta_c^\infty}{\pi} - 2\right)\delta|m_2|.$$

By investigating the characteristic equation for this system, we will find that our stationary cycle is stable in the area given by inequalities (A-23).

ACKNOWLEDGMENTS

The author of the work is grateful to Prof. I.V. Bondar, D. Sci. (Biology), the Head of the Laboratory of Physiology of Sensory Systems (Institute of Higher Nervous Activity and Neurophysiology, Russian Academy of Sciences) for his assistance in writing the article.

REFERENCES

1. D. H. Hubel and T. N. Wiesel, J. Physiol. **160**, 106 (1962).
2. D. Z. Jin, V. Dragoi, M. Sur, and H. S. Seung, J. Neurophysiol. **94** (6), 4038 (2005).
3. W. Wu, P. H. Tiesinga, T. R. Tucker, et al., J. Neurosci. **31** (36), 12767 (2011).
4. N. Nortmann, S. Rekauzke, S. Onat, et al., Cereb. Cortex **25** (6), 1427 (2015).
5. A. Benucci, D. L. Ringach, and M. Carandini, Nat. Neurosci. **12** (10), 1317 (2009).
6. I. A. Shevelev, G. A. Sharaev, N. A. Lazareva, et al., Neuroscience **56** (4), 865 (1993).
7. I. A. Shevelev, U. T. Eysel, N. A. Lazareva, and G. A. Sharaev, Neuroscience **84** (1), 11 (1998).
8. E. D. Gershon, M. C. Wiener, P. E. Latham, and B. J. Richmond, J. Neurophysiol. **79** (3), 1135 (1998).
9. N. A. Lazareva, D. Yu. Tsutskiridze, I. A. Shevelev, et al., Zh. Vyssh. Nerv. Deyat. **53** (6), 722 (2003).
10. N. A. Lazareva, S. A. Kozhukhov, R. S. Ivanov, et al., Zh. Vyssh. Nerv. Deyat. **63** (2), 205 (2013).
11. M. Mulas, S. Pojoga, and V. Dragoi, SfN Abstr. No. 160.17.
12. S. A. Kozhukhov, K. A. Saltykov, and N. A. Lazareva, Zh. Vyssh. Nerv. Deyat. **66** (1), 36 (2016).
13. D. J. Richmond and L. M. Optican, J. Neurophysiol. **64** (2): 370 (1990).
14. A. Benucci, R. A. Frazor, and M. Carandini, Neuron **55** (1), 103 (2007).
15. I. Nauhaus, L. Busse, D. L. Ringach, and M. Carandini, J. Neurosci. **32** (9), 3088 (2012).
16. L. Muller and A. Destexhe, J. Physiol. (Paris) 106 (5–6), 222 (2012).
17. P. C. Bressloff and M. A. Webber, J. Comput. Neurosci. **32** (2), 233 (2012).
18. R. Malach, Y. Amir, M. Harel, and A. Grinvald, Proc. Natl. Acad. Sci. U. S. A. **90** (22), 10469 (1993).
19. W. H. Bosking, Y. Zhang, B. Schofield, and D. Fitzpatrick, J. Neurosci. **17** (6), 2112 (1997).
20. A. Stepanyantz, J. A. Hirsch, L. M. Martinez, et al., Cereb. Cortex **18** (1), 2008.
21. K. A. Martin, S. Roth, and E. S. Rusch, Nat. Commun. **5**, 5252 (2014).
22. R. Miikulainen, J. A. Bednar, Y. Choe, and J. Siroch, *Computational Maps in the Visual Cortex* (Springer Science, 2005).
23. R. Ben-Yishai, R. L. Bar-Or, and H. Sompolinsky, Proc. Natl. Acad. Sci. U. S. A. **92** (9), 3844 (1995).
24. P. C. Bressloff and J. D. Cowan, Phys. Rev. Lett. **88** (7), 078102 (2002).
25. J. Schummers, B. Cronin, K. Wimmer, et al., Front. Neurosci. **1** (1), 145 (2007).
26. A. V. Chizhov, J. Comput. Neurosci. **36** (2), 297 (2014).
27. E. Yu. Smirnova and A. V. Chizhov, Biophysics (Moscow) **56** (3), 496 (2011).
28. E. Y. Smirnova, E. A. Chizhkova, and A. V. Chizhov, Biol. Cybern. **109** (4–5), 537 (2015).
29. P. C. Bressloff, J. D. Cowan, M. Golubitsky, et al., Philos. Trans. R. Soc. Lond. B. **356** (1407), 299 (2001).
30. S. He and D. I. MacLeod, Nature **411** (6836), 473 (2001).

Translated by E. Makeeva